Proceedings of the XII International Symposium on Dynamic Problems of Mechanics (DINAME 2007),
Varoto, P. S. and Trindade, M. A. (Editors), ABCM, Ilhabela, SP, Brazil, February 26 - March 2, 2007

STUDY OF THE FLUID-STRUCTURE INTERACTION ON A DYNAMIC PRESSURE CALIBRATION DEVICE

LEPORE F P[1], SANTOS M B[1], and CASTRO R P[2]

[1] Universidade Federal de Uberlândia , FEMEC, Bloco 1M, Campus Santa Mônica, Uberlândia, 38400-902 MG, Brasil

[2] Peugeot Citroen do Brasil, Estrada Renato Monteiro , s/nº, Porto Real, 27570-000, RJ, Brasil

Abstract: The study of the fluid-structure interaction occurring in static and dynamic pressure calibration system is presented. The device structure is a vertical pressure vessel, completely filled with liquid, and composed by a rigid tube closed at its both ends by flexible circular membranes. The lower membrane is used to apply static or dynamic excitation to the system, while the upper membrane acts as a reference pressure sensor. A finite element model is formulated to represent the coupled field problem. This is a simple model that uses the acoustic wave formulation at the fluid domain and an element with three degree of freedom. At the common mesh interfaces the fluid pressure is converted to forces applied to the structure, and the structural motions produce an effective loading at the fluid domain. Modal and transient analysis are performed and the responses of the displacement at the center of the upper membrane and the pressure at the face of the sensor to be calibrated are calculated for impulsive and harmonic excitations applied at the center of the lower membrane. Tests are conducted on an experimental device. The velocity at the center of the upper membrane is measured by a laser vibrometer, a piezoelectric load cell measures the excitation force, and a piezoresistive transducer measures the pressure. The obtained results are used to validate the static and the dynamic behavior of the proposed computational models. The influence of the pressure vessel geometric parameters on its operational frequency band is also analyzed.

Keywords: dynamic pressure, fluid-structure interaction, acoustic wave

NOMENCLATURE

$[M_e]$ = structural element mass
$[C_e]$ = structural element damping
$[K_e]$ = structural element stiffness
{Fe} = external nodal loads
$\{F_e^{Pr}\}$ = fluid loads at the interface
$\{u_e\}$= structural nodal displacements
$[M_e^P]$ = fluid element mass
$[C_e^P]$ = fluid element damping
$[K_e^P]$ = fluid element stiffness
$[R_e]$ = coupling at the interface
$[M^{fs}]$ = mass coupling at the interface
$[K^{fs}]$ = stiffness coupling at the interface
{Pe} = fluid nodal pressure
SONC = speed of sound in the fluid
DENS = fluid density
Kb = fluid bulk modulus
E = Young modulus
Slim = Limit elastic stress
Smax = maximum Von Mises stress
UYx = displacement at point x
P = fluid internal pressure
Px = pressure at point x
Fx = force measured at point x
FRF = frequency response function
U/F = displacement-force FRF
P/U = pressure-displacement FRF
P/F = pressure-force FRF
Sens = static sensitivity
fn = natural frequency
fexp = experimental frequency result
fsim = simulated frequency result
D = operational frequency band

INTRODUCTION

The measurement of dynamic pressure in fluid flows is required on several engineering applications of the automotive, naval and aerospace industries, medical instrumentation and on several fields of experimental scientific investigation. Most commercial pressure sensors are only statically calibrated, despite their applications be on the measurement of dynamic phenomena, since the dynamic calibration procedures are complex and use expensive experimental devices. (Hjelmgren, 2002) and (Doebelin, 1990).

A pressure vessel filled with fluid generally composes static and dynamic calibration devices, a pressure controlled source and one reference sensor. Their functionality constitutes an special class of a fluid – structure interaction problem, where the external excitations imposed to the elastic structure are transmitted to the fluid domain producing modifications of the velocity and pressure fields, witch retroact on the structure, inducing motions.

The proposed calibration device, shown in Fig. 1, is a cylindrical pressure vessel composed by a rigid tube (d) completely filled with fluid, closed at its extremities by two circular flexible membranes. The upper membrane (c) is used to measure the reference pressure, while the bottom membrane (e) generates the fluid internal pressure when static or dynamic excitations are applied to its center. The mechanical component (f) is used to apply static displacements produced by a micrometric screw. Removing this component, sinusoidal and impulsive excitations can be applied to the center of lower membrane by an electro-dynamic shaker or by an impact hammer. The pressure transducer (a) to be calibrated is installed as near as possible to the upper membrane.

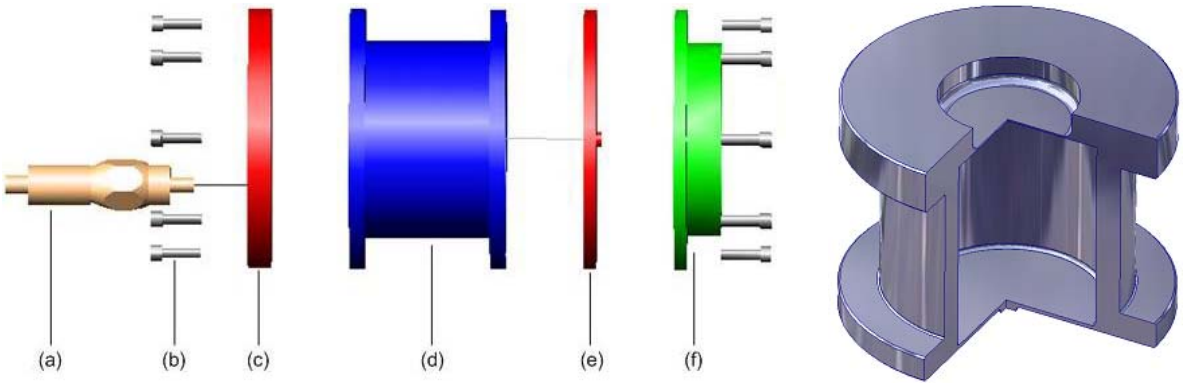

Figure 1 – Prototype of the proposed calibration device

The determination of the vibration modes and the frequency response functions of a flexible structure containing fluid are fundamental to identify the system dynamic behavior. Validated computational models can be used to optimize the design of the calibration device in order to maximize its operating frequency band and to increase its sensitivity.

This paper presents a finite element model formulation to describe the interaction between the internal fluid (water or hydraulic oil) and the elastic structure, considering that the external fluid (air) has negligible viscosity and density properties when compared to those of the internal fluid. Since the internal fluid is confined into a closed domain the acoustic wave propagation theory can be applied to model the dynamic behavior of the calibration device.

A general fluid – structure interaction problem is much more complex than this one. Marand and Ohayon (1995) describe several classes of fluid – structure problems.

Computational simulations were done to calculate the responses of the elastic and fluid domains, due to static and dynamic excitations applied at the centre of the lower membrane. The finite element model numerical results were compared to the experimental responses in order to validate the adopted model and to adjust the internal fluid physical properties and the elastic and geometric parameters of the structure. Finally, the influence of the calibrator geometric parameters on its operational frequency band is analyzed.

FLUID –STRUCTURE INTERACTION: BASIC FORMULATION

The generic system of Fig. 2 represents an elastic structure Ω_S surrounded by an external fluid Ω_F^e and containing an internal fluid Ω_F^i . The structure vibrations at the interfaces induce acoustic waves in both fluid domains. The elastic-acoustic interaction is determined by the simultaneous solution of the appropriated dynamic equations in each domain, and transferring the displacement, velocity and pressure at the interfaces. This procedure has to iterative since the final solution is obtained only if some convergence criterion is fulfilled.

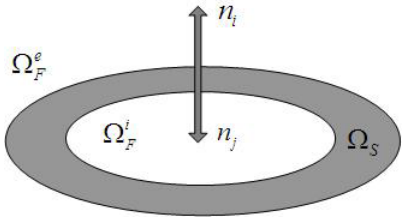

Figure 2 – Elastic structure surrounded by internal and external fluid.

Analytical modeling is not a viable solution for most engineering systems that presents complex geometry. These problems require a domain dicretization and the finite element method constitutes a viable approach to solve the problem.

The mathematical dynamic model of the discretized linear structural domain is represented by a set of ordinary differential equations, as expressed in Eq. 1, for one arbitrary finite element.

$$\left[M_e\right]\left\{\ddot{u}_e\right\}+\left[C_e\right]\left\{\dot{u}_e\right\}+\left[K_e\right]\left\{u_e\right\}=\left\{F_e\right\}+\left\{F_e^{\mathrm{Pr}}\right\} \tag{1}$$

The vector $\{F_e^{Pr}\}$ includes the nodal forces calculated by integrating the fluid pressure over the area of the fluid – structure interfaces. Inside the structure this vector is null.

Generally, in the fluid domain the velocities are obtained from the conservation of momentum principle, and the pressure is obtained from the conservation of mass principle while energy conservation is used to calculate the temperatures. The equations that relate pressure, velocity, temperature, viscosity and density on this domain are solved sequentially, since the flow problem is nonlinear and the governing equations are coupled together.

The proposed calibrator structure flexibility is located mainly at the upper and lower membranes, since the cylindrical tube may be considered rigid in the frequency band bellow 10KHz. Considering that the internal fluid is confined to the structure and that the external fluid viscosity and density are very low, the fluid domain can be represented by a model of acoustic wave propagation, assuming the following additional hypothesis: a) the fluid is compressible and inviscid; b) the fluid mean flow is null; c) the mean density and pressure are uniform throughout the fluid domain. The equations for an arbitrary finite element in the fluid domain is shown in Eq.2 including the dissipation at the interfaces (second term) and the fluid – structure coupling (last term).

$$\left[M_e^P\right]\left\{\ddot{P}_e\right\}+\left[C_e^P\right]\left\{\dot{P}_e\right\}+\left[K_e^P\right]\left\{P_e\right\}+\rho_0\left[R_e\right]^T\left\{\ddot{u}_e\right\}=\left\{0\right\} \tag{2}$$

The coupling term relates the pressure and the nodal forces at the interfaces as expressed by Eq.3.

$$\left\{F_e^{\mathrm{Pr}}\right\}=\left[R_e\right]\left\{P_e\right\} \tag{3}$$

Using these three previous equations, it follows:

$$\begin{bmatrix}\left[M_e\right] & \left[0\right]\\ \left[M^{fs}\right] & \left[M_e^P\right]\end{bmatrix}\begin{Bmatrix}\left\{\ddot{u}_e\right\}\\ \left\{\ddot{P}_e\right\}\end{Bmatrix}+\begin{bmatrix}\left[C_e\right] & \left[0\right]\\ \left[0\right] & \left[C_e^P\right]\end{bmatrix}\begin{Bmatrix}\left\{\dot{u}_e\right\}\\ \left\{\dot{P}_e\right\}\end{Bmatrix}+\begin{bmatrix}\left[K_e\right] & \left[K^{fs}\right]\\ \left[0\right] & \left[K_e^P\right]\end{bmatrix}\begin{Bmatrix}\left\{u_e\right\}\\ \left\{P_e\right\}\end{Bmatrix}=\begin{Bmatrix}\left\{F_e\right\}\\ \left\{0\right\}\end{Bmatrix} \tag{4}$$

where: $\left[M^{fs}\right]=\rho_0\left[R_e\right]^T$ and $\left[K^{fs}\right]=-\left[R_e\right]$ represent the coupling between the pressure and the displacement at the interfaces.

The complete model equation (Castro R P, 2005) is obtained after assembling all finite elements, and has the form of Eq.4, without the subscript (e). The state vector $\left\{u \quad P\right\}^T$ represents the pressure and displacement variables at the model nodes. It should be noted that at those nodes outside the interfaces, the coupling term is zero.

COMPUTATONAL SIMULATION AND EXPERIMENTAL PROCEDURES

The pressure dynamic calibrator finite element mesh and its geometric parameters are shown in Fig.3. The fluid and structural elements are axisymmetric, and the reference frame axis X is in the radial direction and Y is vertical. The computational model was built with the software ANSYS®, using 788 elements PLANE42 (four nodes, displacements UX and UY at each node) to represent the structural domain. The fluid domain is discretized with the 968 elements FLUID29 (four nodes, displacements UX, UY and Pressure at each node). At the nodes of the internal fluid elements (red) the displacement degree of freedom were locked, except those at interface (blue). The fluid-structure coupling was applied at the solid/fluid interface using ANSYS FSI flag. The dominant wavelength in the fluid domain is equal to 59 mm and contains at least 11 elements.

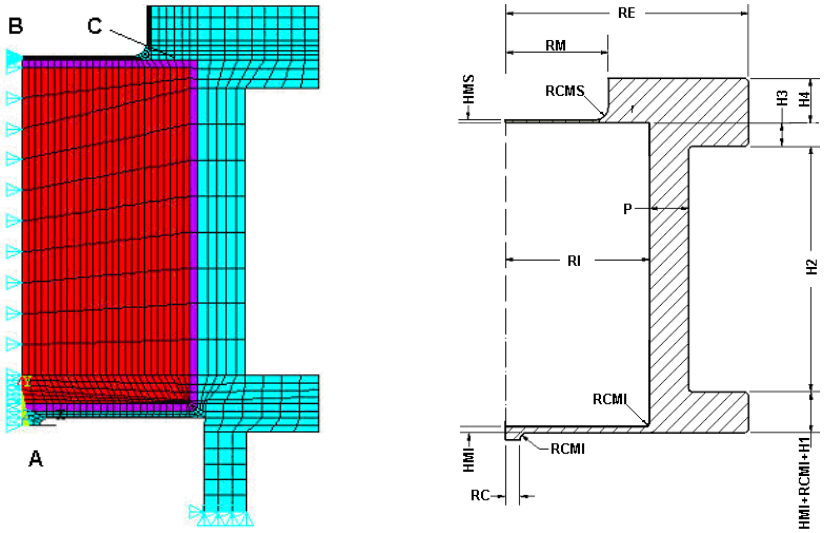

Figure 3 – Finite element model and the device geometric parameters

The points A and B are located at the centers of the lower and upper membranes, and C is the pressure transducer installation point. The axisymmetry condition is applied along the line AB, and the lower flange is fixed, preventing rigid motions of the system. All boundary conditions are represented by the small triangles. Table 1 presents the geometric characteristics of the calibrator device and the structure and fluid properties used in all computational simulations.

Table 1 – Dimensions and physical properties

Parameter	Description	Value
RC	Lower membrane core radius	5 mm
RCMI	Lower membrane fillet radius	2 mm
HMI	Lower membrane thickness	1.89 mm
RI	Lower membrane main radius	48.95 mm
P	Tube wall thickness	13.4 mm
H1	Lower flange thickness	10 mm
H2	Tube length	83 mm
H3	Fraction of the upper flange thickness	8 mm
H4	Fraction of the upper flange thickness	15 mm
HMS	Upper membrane thickness	0.93 mm
RCMS	Upper membrane fillet radius	4.475 mm
RM	Upper membrane main radius	35.035 mm
RE	Flange radius	82.5 mm
ρ_{Steel}	Steel density (SAE 4340)	7890 Kg/m3
E_{Steel}	Young modulus (SAE 4340)	$2.1x10^{11}$ Pa
ν_{Steel}	Poisson ratio (SAE 4340)	0.3
S_{lim}	Limit of elastic stress (SAE4340)	201 MPa
ρ_{Fluid}	Fluid density	800 Kg/m^3
C_{fluid}	Speed of sound in the fluid	1160 m/s

Numerical simulations were done with the computational model as follows: a) Static analysis of the structure submitted to increasing internal pressure, to determine the static load capacity of the device, the linear displacement range of the point B, and the stress state on the structure; b) modal analysis of the structure without internal fluid, to calculate natural frequencies and vibration modes; c) dynamic analysis of the device with internal fluid, to characterize the fluid-structure coupling, using the frequency response functions (FRF) of the displacement measured at point B and the fluid pressure measured at point C, due to excitations applied at point A. At this step, the dynamic sensitivity and the linear operational frequency band of the device are determined.

Experimental tests were carried out with the calibrator prototype using the setup presented by Fig. 4. The impulsive excitation is measured by a piezoelectric load cell installed at the top of the hammer (1); the velocities at the membranes centers are measured by a laser vibrometer (8). The piezoresistive pressure transducer located at point C measures the fluid pressure near the upper membrane. All analog signals produced by the sensors are conditioned (4, 6, and 9) and applied to the inputs of the digital analyzer (5). The frequency response and the coherence functions are estimated by averaging 100 samples, with 2048 points in each one (Bendat J S; Piersol A G, 1986). The obtained experimental results are transferred to a microcomputer (10) and an optimization routine is used to estimate the modal parameters of the device.

The results of the computational simulations were compared to those obtained with the experiments. The modal analysis and the FRF of the structure without internal fluid were used to adjust the geometric parameters of the elastic membranes. The values of HMI, RI, HMS, RCMS and RM presented by Table 1 are the results of this procedure. The FRF obtained with the analysis with internal fluid were used to adjust the value of the sound velocity in the fluid and also to evaluate the dynamic characteristics of the calibrator device. To remove the gas bubbles and dissolved air in the fluid, the device was filled using a combination of hydraulic and vacuum pumps and a set of valves. Details of the sequential filling procedure can be found in Castro R P, 2005.

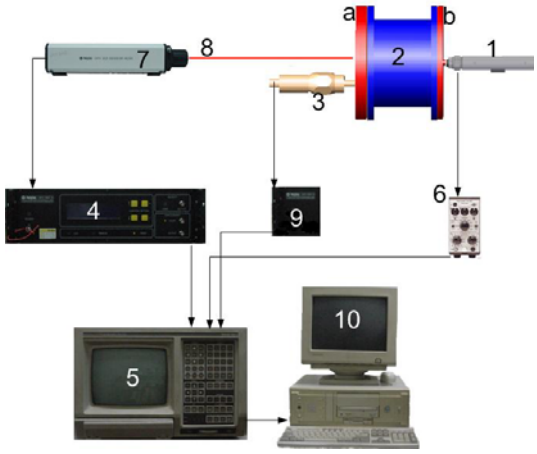

Figure 4 – Instrumentation setup.

SIMULATION AND EXPERIMENTAL RESULTS

The first four modes of the structure finite element model, without internal fluid, are presented by the following figure. It can be seen that bellow 6 KHz the upper and lower vibrations occur mainly at the membranes, and that their modes are uncoupled. This simulation results indicate that the experiments without internal fluid can be done separately on each membrane.

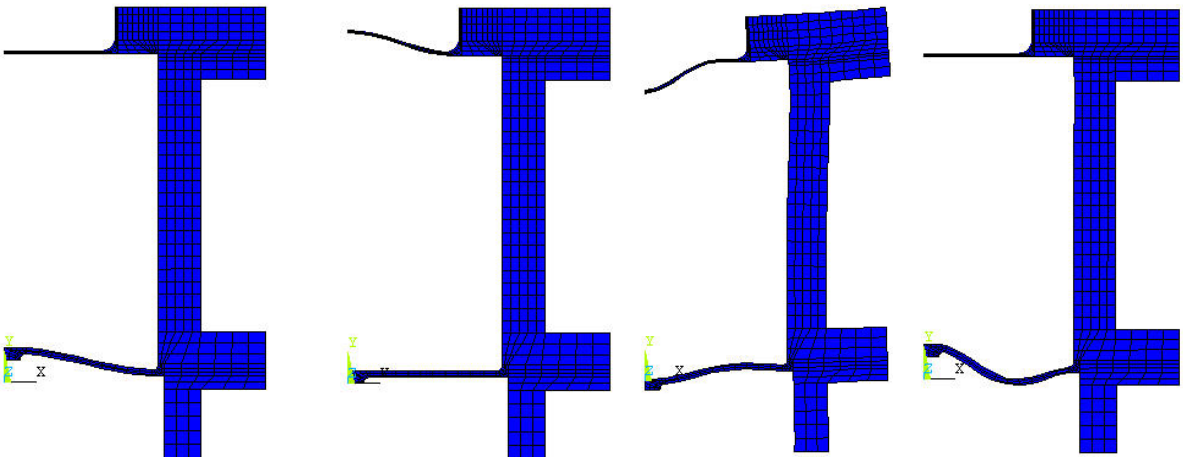

(a) Mode 1: **2014.1 Hz** **(b)** Mode 2: **2270.1 Hz** **(c)** Mode 3: **6436.2 Hz** **(d)** Mode 4: **8052.8 Hz**

Figure 5 – Modes and natural frequencies of the computational model without internal fluid.

Figure 6 shows the comparison of the experimental and simulated FRF for each membrane, in the frequency band from 0 up to 4KHz, where the third and fourth modes are not excited. In both experiments the impulsive excitation was applied to the center of each membrane and the velocity was measured at the same point.

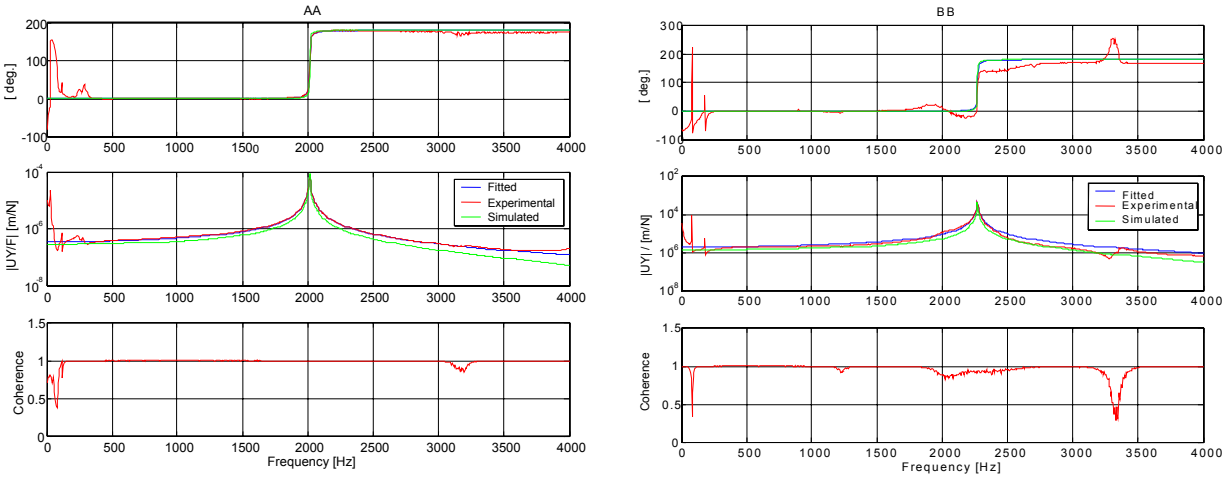

Figure 6 – FRF of the lower (AA) and upper (BB) membranes, without internal fluid.

The fitted curves (blue) were calculated from the experimental data (red), using an optimization procedure that determines the natural frequency and the modal damping factor. The green curves are the results of the harmonic analysis done with the finite element model. The obtained experimental natural frequencies and modal damping factors are: 2014.4 Hz and 0.0027 for the fist mode and 2270.3 Hz and 0.0023 for the second. These frequencies when compared to those shown in Fig. 5 have differences lesser than 0.01%, indicating that the structural finite element model can be used to simulate the device behavior without internal fluid. The higher modes were not identified experimentally; since the device will operate bellow the frequency of the first mode.

The experiments and numeric simulations of the device filled with internal fluid were done to validate the fluid – structure interaction in the finite element model, to adjust the physical and geometrical properties of the fluid, and to define the static and dynamic sensitivities. The pressure transducer to be calibrated is installed near the upper membrane, which is used as a reference. The calibration procedure follows the standard ANSI MC88 1-1972 (Bean, 1993/94).

To determine the experimental static sensitivity of the device increasing displacements were applied to the center (A) of the lower membrane and the displacement (UY) resulting at the center of the upper membrane (B) and the pressure (PC) indicated by the transducer were measured. This transducer is made by IFM Electronic (model PA3024), has 1 MPa linear range and uncertainty equal to 0.7% of the full scale. Figure 7 shows the obtained results.

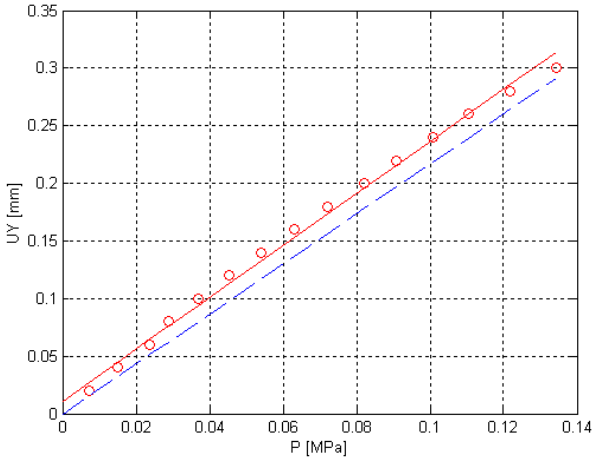

Figure 7 – Static tests: Dashed line = Simulation; (o) = Experimental data; Continuous line = fitted curve.

The experimental static sensitivity equal to 2.166 mm/Mpa, was calculated by linear fitting applied to the measured data pairs (UY, P), while the simulation resulted 2.256 mm/Mpa. The 3.98 % difference may be caused by the uncertainty of the pressure transducer and also due to variance of the upper membrane thickness along its radius. The machining process causes this last effect: the cutting tool produces elastic deformations of the thin membrane, which results thicker at the center than at the outer radius. The finite element model uses a mean value of HMS= 0.93 mm, adjusted by the modal experiments of the device without internal fluid. Another possible source of error is the adopted value of the fluid bulk modulus, which changes with the amount of gas dissolved in the fluid. All these error sources were not experimentally quantified.

The finite element with internal fluid is used to determine the pressure field in the fluid and the mode shapes. The FRF of the displacement measured at (B) and the pressure measured at (C) due to an excitation applied at (A) are calculated in dynamic experiments and also simulated by the device model.

The fluid density and the bulk modulus (Kb) values have significant influence on the natural frequencies of the vibration modes. The DENS and SONC parameters in the finite element program specify them. The amount of bubbles and dissolved gas fraction in the fluid has minor effect on its density but has large effect on its compressibility, which reflects on the SONC value that depends on the Kb value.

The adopted values for these parameters are SONC = 1115 m/s^2, DENS = 800 Kg/m^3 and Kb = $1.49.10^9$ N/m^2, which produce the best agreement between the experimental and simulated natural frequencies of the first two modes.

Figure 8 shows the first two modes of the computational model with internal fluid. The main observed characteristics of these modes are the phase difference of the membranes movements and the pressure field distribution. In the first mode the membrane motions are in phase and the fluid pressure goes from negative value at the upper membrane to positive at the lower one. The second mode shows out of phase motions at the membranes and the pressure distribution has negative values in the middle region of the model height and positive values near the membrane faces.

The presence of the internal fluid couples the membrane movements. This explains the differences between these mode shapes and those obtained for the structure without internal fluid, presented by Fig. 5. As can be seen in Fig. 8, the cylindrical tube structure may be considered as rigid even at the second vibration mode.

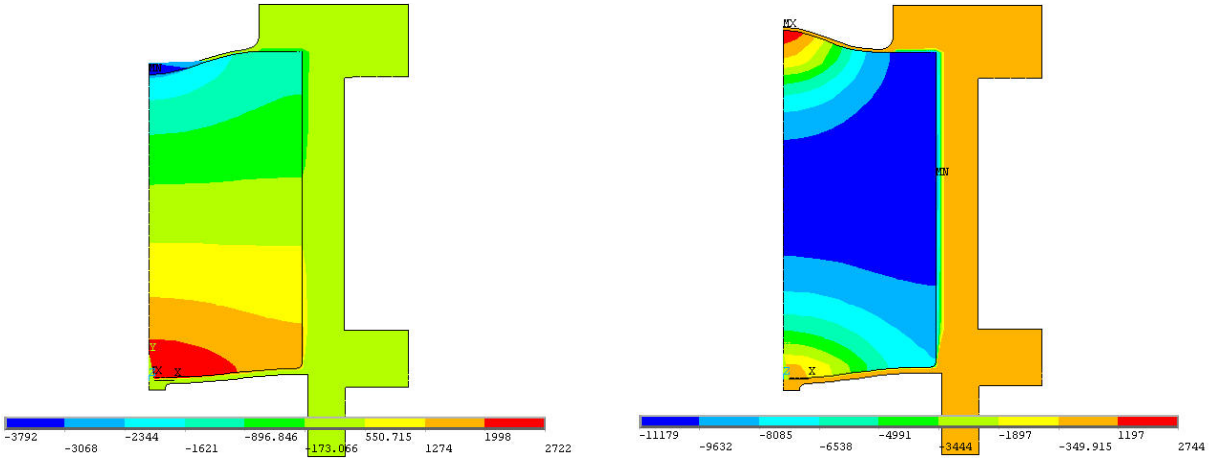

Mode 1: **1240 Hz** Mode 2: **3150 Hz**

Figure 8 – Computational simulation results: mode shapes and pressure distribution [Pa]

Figure 9 presents the experimental and the computational FRF of the device with internal fluid, relating the displacement at point B, the pressure at point C and the excitation applied at point A, respectively, UYB/FA, PC/UYB. Table 2 presents the natural frequencies and the modal damping factors of the two first modes identified from the experimental results of Fig. 9, in the 0 – 4Khz frequency band, and compare then with the simulation results.

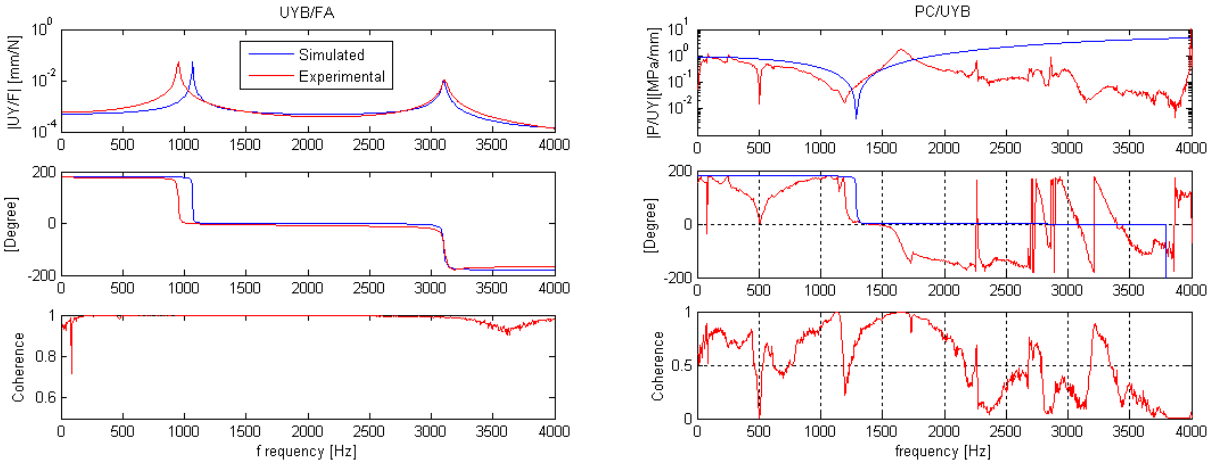

Figure 9 – Comparison of the experimental and simulated frequency response functions, with internal fluid.

Table 2 – Natural frequencies and damping factors of the calibrator device with internal fluid.

Modes	f_{exp} [Hz]	Damping factor	f_{sim} [Hz]	Diff. [%]
Mode 1	950.5	0.0063	1064.6	12.00
Mode 2	3109.5	0.0055	3102.4	-0.23

The 12% difference of the first mode frequency indicates that the finite element model is stiffer than the experimental device. At the first mode shape, shown by Fig. 8, there is significant moment loading on the region that connects the membranes to the flanges of the cylindrical tube. The finite element model assumes no discontinuity at these regions, while in the experimental device the connections are done by 8 circumferentially distributed screws that press rubber o-rings between the membranes and tube flanges. These kinds of fixtures add some additional flexibility to the structure, which can be responsible for the reduction of the first natural frequency.

It should be noted that the dynamical behavior of the pressure transducers is unknown (the manufacturer has no information and no reference dynamic pressure transducer was accessible for comparison). This may explain the discrepancies between simulated and experimental FRF that represents PC/UYB as shown at the right of Fig. 9. Reasonable agreement in the FRF modulus and phase is found in the frequency band bellow 400 Hz, where the coherence has mean value of 75%. Above this frequency the computational model cannot be validated. A new experiment was done at the 0 to 400 Hz frequency band, keeping the same acquisition settings of the previous tests. The resolution of 0.5 Hz improves the coherence function values. The resulting PC/UYB FRF is shown in Fig. 10.

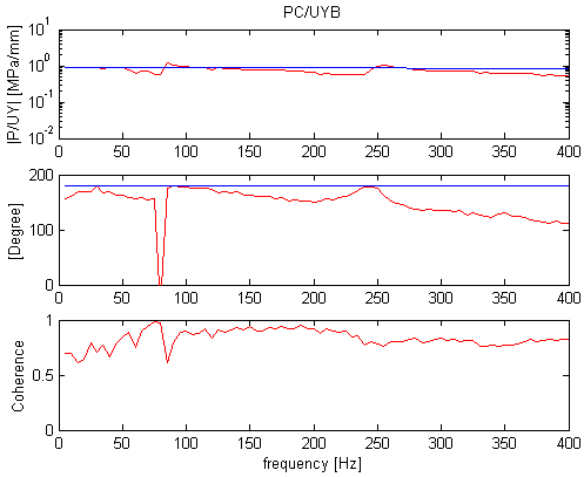

Figure 10 –Frequency response functions, with internal fluid, at the 0-400Hz frequency band.

Assuming PC/UYB obtained in the simulations of the computational model as reference, the pressure transducer model PA3024 can be calibrated. The data in Fig. (10) indicates a maximum gain error equal to 14.3 % and a mean shift of –30.8 degrees. The most significant phase difference occurs at 80 Hz, where the coherence is 1, indicating a possible resonance. This analysis can be used to define the transducer operational frequency band upper limit in function of the acceptable gain and phase errors.

Transient analysis was done with the finite element model. Figure 11a shows the time domain results (UYA, UYB and PB) and Figure 11b presents the peak amplitudes along the upper membrane radius, for an imposed harmonic excitation with amplitude UYA = 0.3 mm at 100 Hz.

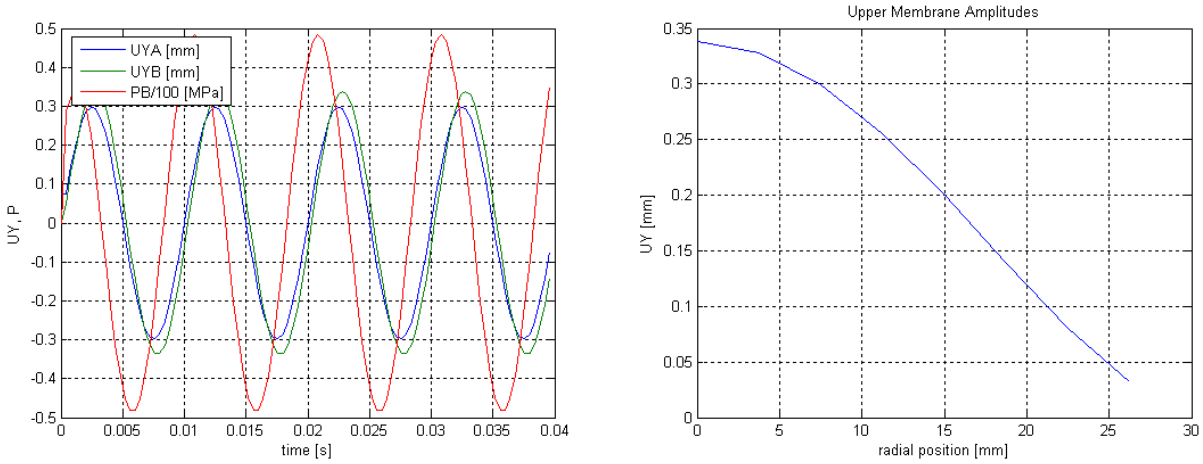

Figure 11 – Simulation of harmonic excitation: a) time domain displacements (UYA, UYB) and pressure (PB) and b) upper membrane displacements in the radial direction.

DESIGN RECOMMENDATIONS AND CONCLUSIONS

The computational model was used to analyze the influence of the structural geometric parameters of the device in order to improve its static sensitivity (Sens) and the operational frequency band (D) that depends on the value of the natural frequency of the first mode. For the device proposed configuration, the upper membrane governs the static sensitivity and the load capacity.

Two optimization problems are defined: 1) for a given pressure (P), adjust (HMS, RM and RCMS) to maximize Sens, restricting the maximum stress (Smax) to the material yield limit (Slim); 2) for a given pressure (P), adjust (HMI, RI, RCMI and H2) to maximize the value of the device first natural frequency (fn), restricting the nonlinearity level and the phase shift in the frequency band.

To exemplify, a calibration device made of ANSI 4340 steel was designed with full scale equal to 1 Mpa and Slim= 400 Mpa. The first optimization problem solution results are: the relation RM/HMS = 28.65, the fillet radius RCMS=5 mm for a maximum value Sens/HMS = 0.548 Mpa^{-1}, when the lower membrane parameters were fixed to RI = 50 mm, HMI = 2 mm and RCMI = 2 mm. The second optimization problem was solved for 1% dynamic uncertainty and phase

difference lesser than 1 degree, resulting: H2 = 20 mm and Sens = 0.547Mpa/mm. The first natural frequency is 2208.8 Hz and the frequency band is limited to 240 Hz. Sampled values of the optimization process are included in Tab. 3.

Table 3 – Influence of the geometric parameters on the dynamic behavior of the device.

Dimensions [mm]	H2 = 80			H2 = 40			H2 = 20		
	HMS=0.9 RM=25.8	HMS=1.0 RM=28.7	HMS=1.4 RM=40.1	HMS=0.9 RM=25.8	HMS=1.0 RM=28.7	HMS=1.4 RM=40.1	HMS=0.9 RM=25.8	HMS=1.0 RM=28.7	HMS=1.4 RM=40.1
f_n [Hz]	1924.6	1778.9	1344.8	2262.9	2042.6	1512.9	2472.9	2208.8	1630.8
Sens [mm/Mpa]	0.438	0.547	0.766	0.438	0.547	0.766	0.438	0.547	0.766
D [Hz]	290	250	180	310	250	180	360	240	208

Increasing the value of HMS (thickness of the upper membrane) reduces the first natural frequency. This result is not contradictory since RM increases proportionally to HMS in order to maintain the stress Smax close to Slim.

The parameter H2 has small effect on the static sensitivity (Sens), but reducing H2 produces higher values of the first natural frequency, which increases the operational frequency band (D), and the pressure distribution becomes uniform in the fluid domain. Consequently, the transducer to be calibrated can be installed at any position of the device surface. The following figures summarize this discussion, using parameterized variables, instead their absolute values.

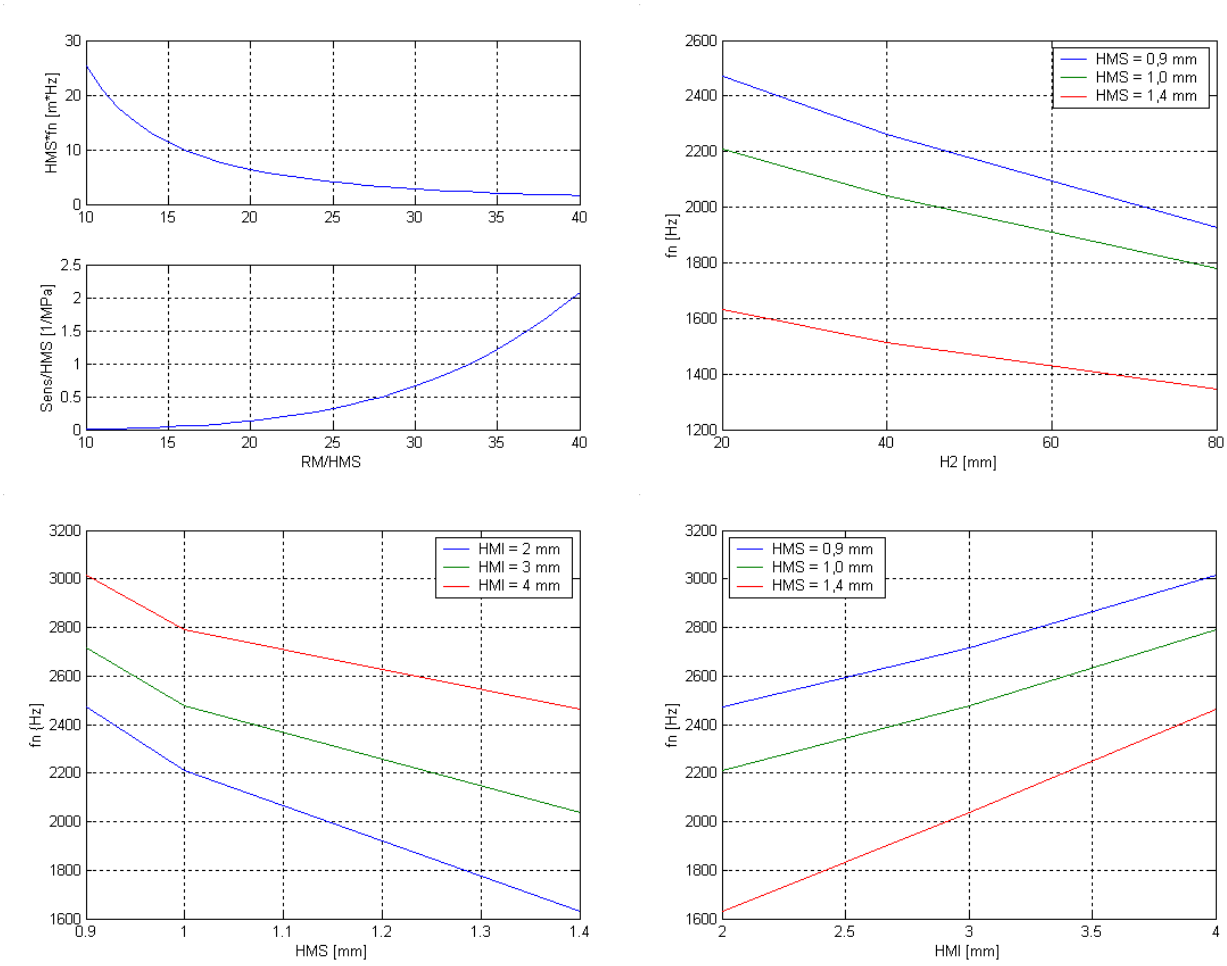

Figure 12 – Geometric parameters influence on the behavior of the calibrator device.

The bottom curve of the upper-left part of Fig. 12 can be used to obtain the RM/HMS relation that produces de desired Sens/HMS sensitivity relation. The upper curve gives the resulting product HMS*fn. This procedure is qualitative since only few points of these curves were sample in the optimization procedures.

The other three curves of Fig. 12 present the influence of the most sensitive parameters (H2, HMS and HMI) on the value of the device first natural frequency.

The ambient temperature variations during an static calibration test produces undesirable drift on the pressure measured by the transducer, since the fluid and the structure volumes changes as consequence of the differences of their thermal expansion coefficients. Long duration experiments must be done in a temperature-controlled environment, and must consider the fluctuation of the atmospheric pressure, to reduce the drift effect. Dynamic tests are unaffected by this low frequency phenomena, because they can be easily conditioned by a band-pass filter that removes the undesirable low and high frequencies of the measured signals.

The proposed configuration of the calibrator device is simple, easy to operate and allows static and dynamic calibration on the same device, without any structural modification. The device full-scale capacity can be modified changing the thicknesses of the upper and lower membranes. The excitation applied to the lower membrane may be done by an impact hammer or by an electro-dynamic shaker for low and moderate pressure amplitudes.

The weakness of the experimental procedure presented by this paper is related to the unknown dynamic characteristics of the pressure transducer made by IFM Electronic (model PA3024). The low values of the coherence functions associated with the easements of the pressure signals may indicate that its operational frequency band is far bellow that used in the experiments.

The solutions obtained with proposed finite element model shown reasonable agreement with the experimental data, mainly for the FRF UYB/FA. This model can be also used to design pressure transducers that use membranes as the sensor element.

The acoustic wave propagation approach is valid since the internal fluid is confined into the structure and the surrounding air effect can be disregarded. Additional modeling approaches are under investigation. One of than includes in the finite element model the hydraulic connector that fixes the pressure transducer to the upper membrane surface. The other one uses a more generic four nodes fluid element (FLUID141) with seven degree of freedom on each node.

ACKNOWLEDGMENTS

Authors acknowledge CNPq for the financial support (grant number 500989/2003-6).

REFERENCES

Castro R. P, 2005; “Projeto e Identificação Experimental de um protótipo de Calibrador de pressão estática e dinâmica”; Dissertação de Mestrado, 129 p, ftp.mecanica.ufu. br /FEMEC/ teses/rpcastroMS.pdf.

Doebelin, E, 1990, ‘Measurement Systems – Application and Design”, 4th edition, McGraw-Hill International editions, ISBN 0-07-017338-9.

Hjelmgren; J., 2002, “Dynamic Measurement of Pressure - A Literature Survey”, SP Swedish National Testing and Research Institute; SP Report 2002-34

Marand, H. J. P., Ohayon, R., 1995, “Fluid-Structure Interaction”, second edition, John Wiley, New York.

RESPONSIBILITY NOTICE

The authors are the only responsible for the printed material included in this paper.